

Boosting CO₂ electroreduction performance over fullerene-modified MOF-545-Co promoted by π - π interaction

Xue Dong^a, Zhifeng Xin^{a,*}, Dong He^a, Jia-Ling Zhang^a, Ya-Qian Lan^{b,c}, Qian-Feng Zhang^a, Yifa Chen^{b,c,**}

^a Institute of Molecular Engineering and Applied Chemistry, Anhui University of Technology, Ma'anshan 243002, China

^b National and Local Joint Engineering Research Center of MPES in High Energy and Safety LIBs, Engineering Research Center of MTEES (Ministry of Education), Key Lab. of ETESPG(GHEI), School of Chemistry, South China Normal University, Guangzhou 510006, China

^c Jiangsu Key Laboratory of New Power Batteries, School of Chemistry and Materials Science, Nanjing Normal University, Nanjing 210023, China

ARTICLE INFO

Article history:

Received 23 February 2022

Revised 30 March 2022

Accepted 22 April 2022

Available online 27 April 2022

Keywords:

Fullerene

Metal organic framework

Electrocatalytic performance

π - π interaction

CO₂RR

ABSTRACT

Metal-organic frameworks (MOFs) have showed high promise in CO₂-electroreduction, yet their generally insufficient conductivity or low electron-transfer efficiency have largely restricted the wide-spread applications. Herein, fullerene molecules (i.e., C₆₀ and C₇₀) have been successfully introduced into the pore-channels of a Co-porphyrin based MOF through a facile strategy. Thus-obtained hybrid materials present higher electron-transfer ability, enhanced CO₂ adsorption-enthalpy and CO₂ electroreduction activity. Notably, the charge transfer resistance (R_{ct}) of C₆₀@MOF-545-Co is almost 5 times lower of than that of MOF-545-Co, as well as 1.5 times increased for the CO₂ adsorption enthalpy. As expected, the FE_{CO} of C₆₀@MOF-545-Co (97.0%) is largely higher than MOF-545-Co (70.2%), C₆₀@MOF-545 (19.4%), C₆₀ (11.5%) and physical mixture (70.3%) and presented as one of the best CO₂ electroreduction catalysts reported in H-cell system. The facile strategy would give rise to new insight into the exploration of powerful MOF-based hybrid materials in high-efficiency CO₂ electroreduction.

© 2023 Published by Elsevier B.V. on behalf of Chinese Chemical Society and Institute of Materia Medica, Chinese Academy of Medical Sciences.

In recent years, more and more attention has been attracted to environmental issues all around the world. The waste gas emitted by factories increases the concentration of carbon dioxide, exacerbated the greenhouse effect [1–3]. Many efforts have been devoted to resolve this problem, such as storing CO₂ by biological or mineral means, converting CO₂ into useful chemicals *etc.* Among them, reducing CO₂ into useful fuels through electrochemical methods is a promising approach. Recently, researchers have developed numerous materials [4–6] that could serve as electrocatalysts for electrocatalytic carbon dioxide reduction reaction (CO₂RR) [7–10], such as noble metals [11], metal oxides [12], metal chalcogenides [13–15], metal-free materials [16–19], and porous crystalline materials (e.g., MOFs or COFs) [20–25]. Among these various catalysts, MOFs with sufficient active metal sites, plenty of porosity and efficient mass-transfer ability make them ideal platforms for electrocatalytic CO₂RR, while the low electron transfer ability restricts

the catalytic application in CO₂RR for most of MOFs. In order to further develop the catalytic potential of MOFs, many efforts have been devoted to increase the electron transfer rate in CO₂RR process, such as introducing functional ligands or metal clusters with plenty of delocalized electrons, loading conductive polymers in the channels of MOFs [4,26–29], and so forth. However, the complicated processes of material design and loading methods also limit the wide applications of MOFs in the catalytic CO₂RR [30–33].

Fullerenes have been created great interest in material chemistry owing to their unique cage structure and every carbon atom links with three adjacent carbon atoms through sp²-hybridization [36]. For example, the C₆₀ molecule has a symmetric structure with the diameter of 0.71 nm. In the cage structure, π orbital of fullerene is more out of the cage and the electronic structure has naturally focused on the surface. This highly conjugated π -electron system of hollow carbon cage affords it with electron-acceptor capacities [34–36], and the special structure is beneficial for efficient electron transfer in catalytic process [37,38]. Thus, it would be deduced that the addition of fullerene molecules into MOFs could greatly enhance the electron migration efficiency in the catalytic process [39,40], and interacted with MOF structure with π - π interactions.

* Corresponding author.

** Corresponding author at: National and Local Joint Engineering Research Center of MPES in High Energy and Safety LIBs, Engineering Research Center of MTEES (Ministry of Education), Key Lab. of ETESPG(GHEI), School of Chemistry, South China Normal University, Guangzhou 510006, China.

E-mail addresses: xinzf521@ahut.edu.cn (Z. Xin), chyf927821@163.com (Y. Chen).

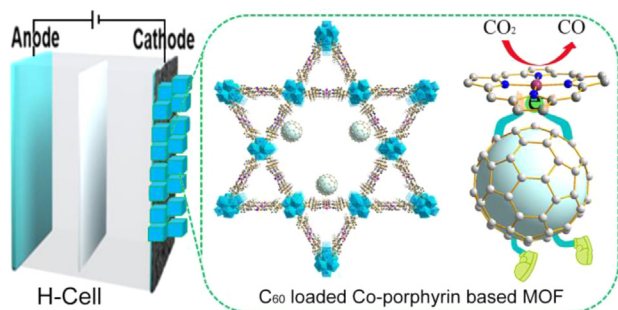


Fig. 1. The schematic illustration of fullerenes loaded MOF composites for electroreduction of CO_2 .

Herein, C_{60} has been introduced into MOFs structure by a one-pot impregnation method. In the structure of C_{60} @MOF-545-Co composite material, the π -electron system of C_{60} might overlap with π -electron system of porphyrin, which would endow MOFs composites with higher electron transfer ability, CO_2 adsorption capability and enhanced catalytic selectivity for CO_2 RR (Fig. 1). Specifically, C_{60} @MOF-545-Co can selectively convert CO_2 to CO with Faradaic efficiency (FE_{CO}) of 97.0% at -0.7 V. The FE_{CO} can also maintain above 90.0% during the electrolysis process in 10 h and the current density of C_{60} @MOF-545-Co remains almost constant. This work might extend the application scope of MOFs as powerful hybrid materials in efficient CO_2 electroreduction.

The detailed synthesis procedures of C_{60} @MOF-545-M and C_{70} @MOF-545-M are list in the following: In a 50 mL Schlenk tube, 50 mg activated MOF-545-Co is added. A solution of C_{60} (8 mg) in 1 mL carbon disulfide (CS_2) is dropped on the MOF-545-Co powder until the solution just submerges the powder. Subsequently, the Schlenk tube is sonicating in ice bath for 1 h, collect the powder and washed with CS_2 until the filter become colorless, after drying under vacuum at 60°C for 8 h, about 54 mg powder is collected. The preparation of C_{60} @MOF-545-Fe or C_{60} @MOF-545-Ni is similar to the procedure C_{60} @MOF-545-Co, except MOF-545-Fe or MOF-545-Ni is used instead of MOF-545-Co, respectively. Simultaneously, C_{70} @MOF-545-Co is also prepared by the similar method using C_{70} as a doping reagent. The hybrid MOF materials with different loading amounts of C_{60} (denoted as C_{60} :CoTCPP = 1:2, C_{60} :CoTCPP = 1:3 and C_{60} :CoTCPP = 1:6) are obtained by controlling the concentration of C_{60} in CS_2 solution.

A new class of C_{60} -doped MOF-545 with enhanced catalytic efficiency is synthesized by a one-pot immersion method [41,42]. In the structure of C_{60} @MOF-545-Co, Zr_6O_8 clusters were linked by Co-TCP ligand to assemble the porous MOF structure [30,43]. Powder X-ray diffraction (PXRD) tests confirm that the structure of C_{60} @MOF-545-Co is consistent with MOF-545-Co, indicating that the implantation of C_{60} have not changed the structure of MOF (Fig. 2a). Nevertheless, the C_{60} peaks are not observed in the PXRD pattern of C_{60} @MOF-545-M, it probably attributed to the uniform dispersion and low loading amount of C_{60} in MOF structure, and no corresponding diffraction peak is formed [44]. To investigate the catalytic performance of C_{60} in MOF with different transition metals, C_{60} molecule is also introduced into both MOF-545-Fe and MOF-545-Ni by the similar procedures. The PXRD patterns (Fig. S1 in Supporting information) demonstrate that C_{60} @MOF-545-Fe and C_{60} @MOF-545-Ni show the similar phase structure of MOF-545. Scanning electron microscope (SEM) tests show that the as-prepared C_{60} @MOF-545-Co displays rod-like morphology [45]. The smooth surface of the rods implies that C_{60} is not loaded on the surface of MOF-545-Co. Specifically, the morphology of C_{60} @MOF-545-Co (Fig. 2d) remained unchanged during the loading process of C_{60} based on MOF-545 (Fig. 2b) and MOF-545-Co (Fig. 2c) [28].

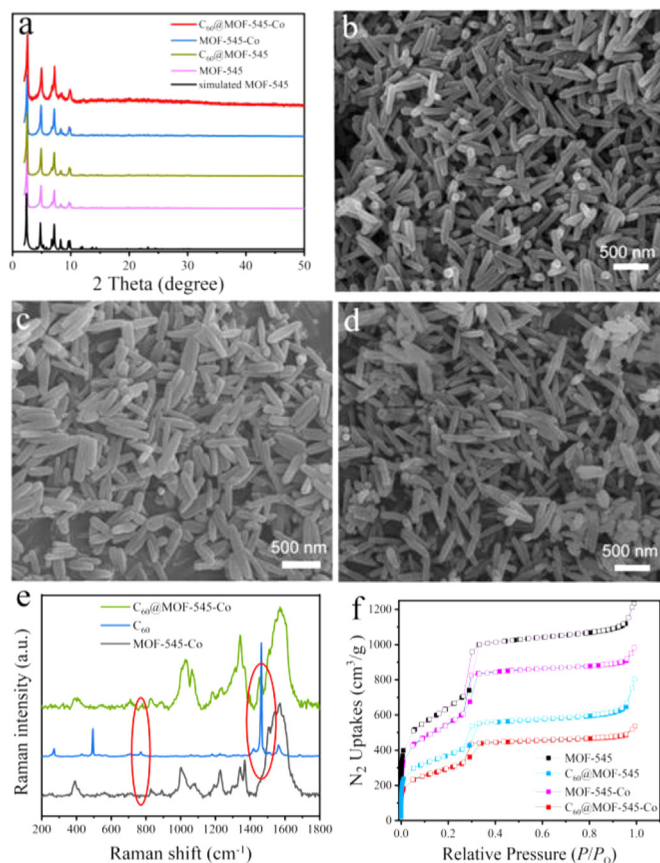


Fig. 2. Characterization of C_{60} @MOF-545-Co. (a) PXRD patterns of C_{60} @MOF-545-Co, MOF-545-Co, C_{60} @MOF-545, MOF-545 and simulated MOF-545. SEM image of (b) MOF-545, (c) MOF-545-Co and (d) C_{60} @MOF-545-Co. (e) Raman spectra of C_{60} @MOF-545-Co, MOF-545-Co and C_{60} . (f) N_2 sorption isotherms of C_{60} @MOF-545-Co, MOF-545-Co, C_{60} @MOF-545 and MOF-545.

Raman spectroscopy is utilized to determine the presence of C_{60} in C_{60} @MOF-545-Co structure (Fig. 2e). Raman spectra display the characteristic peaks of C_{60} corresponding to the typical A_g and H_g vibration modes. For the spectrum of C_{60} , the major bands at 500 and 1471 cm^{-1} correspond to the A_g vibration modes of C_{60} . Other distinct vibration peaks at 271 , 712 , 770 and 1569 cm^{-1} are ascribed to the active H_g vibration modes [46]. Specifically, the Raman spectrum of C_{60} @MOF-545-Co shows obvious peaks at 770 cm^{-1} and 1467 cm^{-1} , which may be attributed to the H_g and A_g vibration modes of C_{60} , respectively. The above result indicates that C_{60} is successfully integrated in C_{60} @MOF-545-Co.

In addition, N_2 sorption tests are conducted to evaluate the porosity of the obtained materials. The Brunauer-Emmett-Teller surface areas (S_{BET}) of MOF-545, C_{60} @MOF-545, MOF-545-Co and C_{60} @MOF-545-Co are calculated to be $2307\text{ m}^2/\text{g}$, $1327\text{ m}^2/\text{g}$, $1957\text{ m}^2/\text{g}$ and $1106\text{ m}^2/\text{g}$, respectively (Fig. 2f and Table S1 in Supporting information). The S_{BET} and total pore volume (V_t) of C_{60} @MOF-545-Co is decreased when compared with that of MOF-545-Co owing to the loading of C_{60} would occupy a part of the pore (Fig. S2 in Supporting information). To further understand the properties of pore structure for the obtained samples, CO_2 adsorption measurements are performed. According to the CO_2 uptake curves (Fig. S4 in Supporting information), the CO_2 adsorption capacities of MOF-545-Co and C_{60} @MOF-545-Co are calculated to be $36\text{ cm}^3/\text{g}$ and $26\text{ cm}^3/\text{g}$ at 298 K and 1 atm , respectively. The decrease of CO_2 uptake would also be attributed to the loading of C_{60} that occupies part of the pore. After calculation, C_{60} @MOF-545-Co can absorb about 9 CO_2 molecules per unit cell at 1 atm and 298 K , which would be

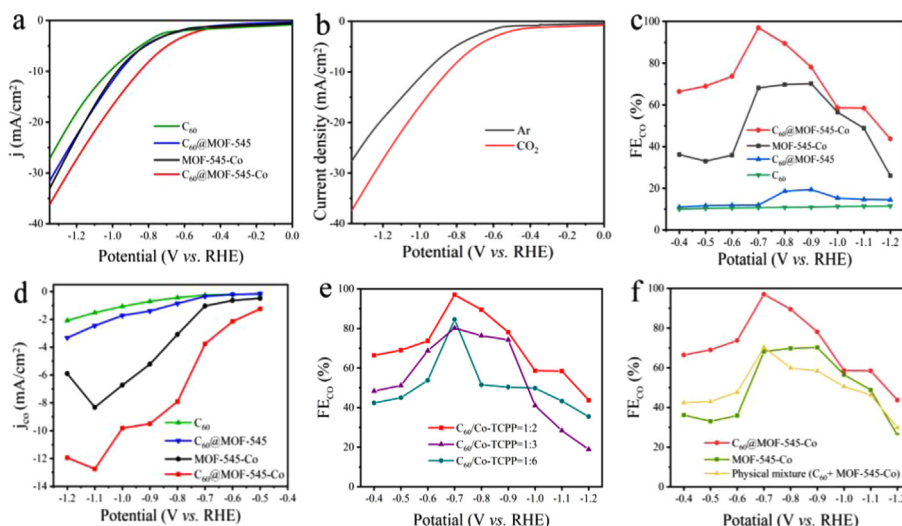


Fig. 3. Electrocatalytic CO₂RR performances: (a) LSV curves of C₆₀@MOF-545-Co and comparison sample. (b) LSV curves of C₆₀@MOF-545-Co in Ar and CO₂ saturated 0.5 mol/L KHCO₃ aqueous solution. (c) Faradaic efficiencies for CO at different potentials. (d) Partial CO current density. (e) FE_{CO} of C₆₀@MOF-545-Co with different C₆₀ loading capacity. (f) FE_{CO} of C₆₀@MOF-545-Co, MOF-545-Co and physical mixture (C₆₀+MOF-545-Co).

beneficial for efficient electrocatalytic CO₂RR. In addition, the adsorption enthalpy of C₆₀@MOF-545-Co and MOF-545-Co (Figs. S3 and S4 in Supporting information) are calculated based on the CO₂ adsorption curves obtained at 273 K, 283 K and 298 K. The CO₂ adsorption enthalpy of C₆₀@MOF-545-Co (32 kJ/mol) is obviously higher than that of MOF-545-Co (23 kJ/mol). The results indicate that the introduction of C₆₀ is beneficial for the enhanced adsorption of CO₂.

The electrocatalytic performance of C₆₀@MOF-545-Co for CO₂RR is measured using three-electrode system in an H-type cell containing CO₂-saturated 0.5 mol/L KHCO₃ (pH 7.2) aqueous solution. Firstly, catalytic selectivity of MOF-545-Co, MOF-545-Fe and MOF-545-Ni is carried out and the corresponding FE_{CO} is evaluated over a wide potential range (from −0.4 V to −1.2 V). MOF-545-Co has a higher FE_{CO} value (70.2%, −0.9 V) than MOF-545-Fe (53.0%, −0.7 V) and MOF-545-Ni (46.4%, −1.0 V), which is similar to the previous reported result (Fig. S5 in Supporting information) [28]. In addition, we also select MOF-545-Co, MOF-545-Ni and MOF-545-Fe to load C₆₀ and further test their catalytic performances. The result indicates that C₆₀@MOF-545-Co (97.0%, −0.7 V) shows higher FE_{CO} value than C₆₀@MOF-545-Fe (68.0%, −0.8 V) and C₆₀@MOF-545-Ni (53.5%, −0.9 V) (Fig. S1 in Supporting information). Therefore, we choose C₆₀ loaded MOF-545-Co as the desired platform for further CO₂RR investigation.

To detailly study the electrocatalytic activity of C₆₀@MOF-545-Co for CO₂RR, a series of contrast samples (*i.e.*, MOF-545-Co, C₆₀ and C₆₀@MOF-545) are prepared to test their specific electrocatalytic performances for comparison. The catalytic activity of C₆₀@MOF-545-Co is preliminarily evaluated using linear sweep voltammetry (LSV) in 0.5 mol/L KHCO₃ electrolyte. LSV curves show that the variation trend of current with the increase of voltage. The largest current density of C₆₀@MOF-545-Co in LSV curve is 37 mA/cm² at −1.37 V, which is obviously higher than that of contrast samples (Fig. 3a). The current density of C₆₀@MOF-545-Co in CO₂-saturated KHCO₃ solution is much higher than that in Ar-saturated KHCO₃ solution, which indicates that the high current density of C₆₀@MOF-545-Co mainly comes from CO₂RR (Fig. 3b) [47]. C₆₀@MOF-545-Co exhibits a smaller onset potential and a larger total current density than MOF-545-Co, C₆₀ and C₆₀@MOF-545, which indicates the high catalytic activity of C₆₀@MOF-545-Co. To study the effect of the C₆₀ introduction on the electron transfer performance, we further test the electronic conductivity

of MOF-545-Co, C₆₀@MOF-545-Co (Fig. S6 in Supporting information). The results show that the electronic conductivity C₆₀@MOF-545-Co is only slightly higher than that of MOF-545-Co, which can be concluded that introducing of C₆₀ can improve the electron conductivity of MOF to some extent and can largely improve the electron transfer efficiency from the catalyst surface to the reactant molecules in the electrocatalysis process. The gaseous and liquid products are detected by gas chromatography (GC) and ¹H nuclear magnetic resonance (NMR) spectroscopy, respectively (Fig. S7 in Supporting information). The result of NMR exhibits that no liquid product has been detected, and the result of GC shows that CO is the main gas product [28,48,49]. Moreover, the FE_{CO} of C₆₀@MOF-545-Co can reach up to 97.0% at −0.7 V, which is largely higher than MOF-545-Co (70.2%), C₆₀@MOF-545 (19.4%) and C₆₀ (11.5%) (Fig. 3c and Fig. S7). This can be concluded that the high catalytic selectivity is originated from the combination of C₆₀ molecules and MOF-545-Co. The CO partial current density of C₆₀@MOF-545-Co (12.7 mA/cm² at −1.1 V) is largely higher than the contrast samples, indicating the better electron transfer ability in the process of CO₂RR (Fig. 3d).

To further study the effect of C₆₀ on the catalytic performance, C₆₀@MOF-545-Co with different C₆₀ loading amounts (*e.g.*, C₆₀:TCPP=1:2, 1:3 and 1:6, respectively) have been prepared and characterized by PXRD and SEM (Figs. S8 and S9 in Supporting information). The results of PXRD and SEM displayed that loading of C₆₀ and the loading amount have not change the crystal structure and morphology of MOF particles. The loading amount of C₆₀ is calculated from the standard curve of UV absorption spectrum [50,51]. The detailed steps are listed in the supporting information (Fig. S10 in Supporting information). Fig. 3e shows the FE_{CO} of C₆₀@MOF-545-Co (1:2) is higher than that of C₆₀@MOF-545-Co (1:3) and C₆₀@MOF-545-Co (1:6), indicating that the higher loading of C₆₀ is benefit for increasing the catalytic performance for CO₂RR. In detail, the FE_{CO} values of them are 97.0% (C₆₀:Co-TCPP=1:2), 84.5% (C₆₀:Co-TCPP=1:3) and 80.2% (C₆₀:Co-TCPP=1:6), respectively. This might be concluded that the loading of C₆₀ in MOF channel can enhance the catalytic efficiency and the optimized C₆₀ loading (C₆₀:Co-TCPP=1:2) with the best performance will serve as be the representative to investigate other properties. To further support the vital role of C₆₀ molecule, we have prepared the physical mixture of MOF-545-Co and C₆₀ (C₆₀+MOF-545-Co with the ratio of C₆₀:Co-TCPP=1:2) (Fig. 3f) and

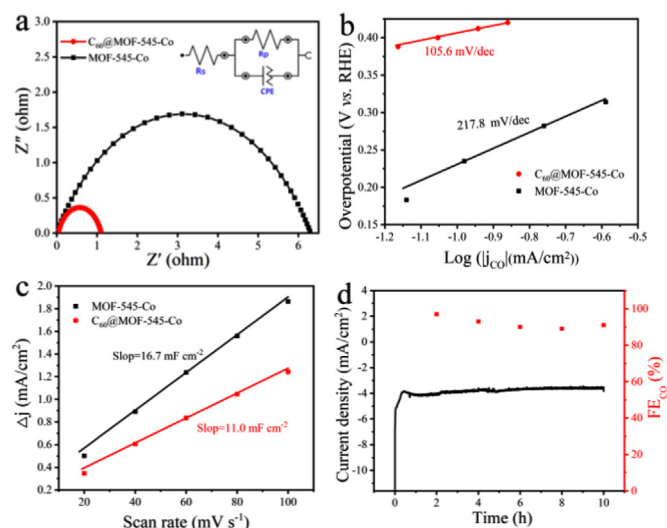


Fig. 4. (a) Nyquist plots, (b) Tafel plots and (c) C_{dl} of C_{60} @MOF-545-Co and MOF-545-Co. (d) Long-term stability of C_{60} @MOF-545-Co at -0.7 V for 10 h.

tested their electrocatalytic performances for CO_2RR . The result shows the lower catalytic performance of physical mixture (70.3%, -0.7 V) than that of C_{60} @MOF-545-Co (97.0%, -0.7 V), which can be concluded that C_{60} can enhance the electron transfer efficiency for CO_2RR in the channel of MOF. Furthermore, the corresponding maximum FE_{CO} of C_{60} @MOF-545-Co, MOF-545-Co, C_{60} @MOF-545 and C_{60} is 97.0%, 70.2%, 19.4% and 11.5%, respectively, proving the vital role of C_{60} in the electrocatalytic CO_2RR (Fig. S11 in Supporting information). In electrocatalysis process, electrochemical impedance spectroscopy (EIS) is usually used to study the hindrance received during the transfer of electrons from the catalyst surface to CO_2 molecules. Nyquist plots are obtained via EIS. Based on the fitted data via Zview software (Fig. 4a), the charge transfer resistance (R_{ct}) of C_{60} @MOF-545-Co (1.14Ω) is five times decreased when compared with that of MOF-545-Co (6.50Ω), proving that the introduction of C_{60} can largely reduce the charge transfer barrier during the electrolysis process.

In the electrochemical process, the polarization of the electrode reflects the obstruction of the electrode process. The Tafel slope is usually used to characterize the performance of electrochemical catalysts because it quantifies the amount of additional applied potential required to observe the logarithmic increase in the measured current. Besides, Tafel slope for C_{60} @MOF-545-Co (105.6 mV/dec) is also largely decreased compared to that of MOF-545-Co (217.8 mV/dec), implying the more favorable kinetics of C_{60} @MOF-545-Co for the CO formation (Fig. 4b).

To further investigate the intrinsic activity of C_{60} @MOF-545-Co and MOF-545-Co, cyclic voltammetry (CV) measurements at different scan rates (Fig. S12 in Supporting information) are applied to evaluate their electrochemical active surface area (ECSA) according to the double-layer capacitance (C_{dl}). The ECSA of C_{60} @MOF-545-Co and MOF-545-Co is calculated to be 275 and 417.5 cm^2 , respectively, based on the value of double-layer capacitance (C_{dl}) (Fig. 4c). Besides, the measured ECSA corrected CO partial current density for C_{60} @MOF-545-Co is 2 times increased after the loading of C_{60} (Fig. S13 in Supporting information), implying that the addition of C_{60} can largely improve the catalytic activity of MOF-545-Co for CO_2RR [52].

The excellent electrocatalytic performance of C_{60} @MOF-545-Co for CO_2RR encourages us to evaluate its stability. The durability test of C_{60} @MOF-545-Co is carried out at -0.7 V in CO_2 -saturated $KHCO_3$ aqueous solution. The FE_{CO} can also maintain above 90.0% during the electrolysis process in 10 h and the current

density of C_{60} @MOF-545-Co remains almost constant (Fig. 4d). The resulting PXRD pattern shows that C_{60} @MOF-545-Co still maintains the origin structure after electrocatalysis for 10 h. Besides, SEM test demonstrates that the morphology of C_{60} @MOF-545-Co keeps unchanged after the CO_2 electrocatalytic reaction. Therefore, C_{60} @MOF-545-Co shows high stability in the process of electrocatalytic reaction (Fig. S14 in Supporting information).

Except for C_{60} , other fullerene like C_{70} has also been studied to explore the versatility of this strategy. C_{70} is also one of the most famous members the family of closed-cage molecules [53–55], and there are similar chemical bonds in C_{60} and C_{70} . In view of the above C_{60} loaded in the pore channel of MOF-545-Co exhibits superior catalytic properties in CO_2RR , C_{70} @MOF-545-Co has been prepared following the similar methods. The PXRD tests confirm that the structure of MOF-545-Co remains unchanged after the loading of C_{70} (Fig. S16a in Supporting information). The SEM image displays the rod-like morphology (Fig. S15a in Supporting information), which is similar to that of C_{60} @MOF-545-Co. In addition, Raman spectroscopy has been utilized to determine the presence of C_{70} in the structure of MOF-545-Co and two obvious peaks detected at 258 cm^{-1} and 768 cm^{-1} can be ascribed to the A_1' and E_2' or E_1'' vibration modes of C_{70} , respectively (Fig. S15b in Supporting information). Compared with the Raman spectroscopy of MOF-545-Co, the Raman spectroscopy of C_{70} @MOF-545-Co shows not only the character peaks of MOF-545-Co but also the peaks of C_{70} , two obvious peaks at 258 cm^{-1} and 768 cm^{-1} correspond to the A_1' and E_2' or E_1'' vibration modes of C_{70} , respectively [56,57]. To further detect the CO_2RR selectivity of C_{70} @MOF-545-Co, the FE_{CO} tests are carried out. As shown in (Fig. S16b (Supporting information), the FE_{CO} for C_{70} @MOF-545-Co (91.1%, -0.8 V) is lower than C_{60} @MOF-545-Co (97.0%, -0.7 V). As we can see from the LSV comparison curves (Fig. S16c in Supporting information), the total current density of C_{70} @MOF-545-Co (35.6 mA/cm^2) is also slightly lower than C_{60} @MOF-545-Co (37 mA/cm^2). EIS measurement further validates this fact, because C_{60} @MOF-545-Co (1.14Ω) has smaller charge transfer resistance than C_{70} @MOF-545-Co (1.21Ω) (Fig. S16d in Supporting information). According to the above results, C_{60} @MOF-545-Co exhibits better catalytic performance for CO_2RR than that of C_{70} @MOF-545-Co.

In summary, fullerene molecules (i.e., C_{60} and C_{70}) have been successfully introduced into the pore-channels of Co-porphyrin based MOF utilizing direct impregnation method. Thus-obtained hybrid materials present higher electron-transfer ability, CO_2 adsorption-enthalpy and enhanced CO_2 electroreduction activity owing to the possibly overlapped π -electron systems of fullerene molecules with Co-porphyrin. Notably, the R_{ct} of C_{60} @MOF-545-Co is almost 5 times lower of than that of MOF-545-Co, as well as 1.5 times increased for the CO_2 adsorption enthalpy. Specifically, C_{60} @MOF-545-Co can selectively convert CO_2 to CO with a high FE_{CO} of 97.0% at -0.7 V, which is largely higher than MOF-545-Co (70.2%), C_{60} @MOF-545 (19.4%), C_{60} (11.5%) and physical mixture (70.3%) and presented as one of the best CO_2 electroreduction catalysts reported in H-cell system. This work would shed light on the exploration of the hybridization of fullerenes and MOFs as powerful hybrid materials in efficient CO_2 electroreduction.

Declaration of competing interest

The authors declare that they have no known competing financial interests or personal relationships that could have appeared to influence the work reported in this paper.

Acknowledgments

This work was financially supported by the National Natural Science Foundation of China (Nos. 22171139 and 21901122);

Natural Science Foundation of Educational Commission of Anhui Province of China (No. KJ2020A0240); the Natural Science Research of Jiangsu Higher Education Institutions of China (No. 19KJB150011) and Project funded by China Postdoctoral Science Foundation (No. 2019M651873).

Supplementary materials

Supplementary material associated with this article can be found, in the online version, at doi:[10.1016/j.ccl.2022.04.057](https://doi.org/10.1016/j.ccl.2022.04.057).

References

- [1] D. Shakun, P.U. Clark, F. He, et al., *Nature* 484 (2012) 49–54.
- [2] J. Qiao, Y. Liu, F. Hong, J. Zhang, *Chem. Soc. Rev.* 43 (2014) 631–675.
- [3] N. Mac Dowell, P.S. Fennell, N. Shah, G.C. Maitland, *Nat. Clim. Change* 7 (2017) 243–249.
- [4] Z. Xin, Y.R. Wang, Y. Chen, et al., *Nano Energy* 67 (2020) 104233.
- [5] D.L. Meng, M.D. Zhang, D.H. Si, *Angew. Chem. Int. Ed.* 60 (2021) 25485–25492.
- [6] C. Chen, X. Yan, S. Liu, et al., *Angew. Chem. Int. Ed.* 59 (2020) 16459–16464.
- [7] D.L.T. Nguyen, Y. Kim, Y.J. Hwang, D.H. Won, *Carbon Energy* 2 (2020) 72–98.
- [8] R. Lin, X. Ma, W.C. Cheong, et al., *Nano Res.* 12 (2019) 2866–2871.
- [9] Y. Zhang, L. Jiao, W. Yang, C. Xie, H.L. Jiang, *Angew. Chem. Int. Ed.* 60 (2021) 7607–7611.
- [10] Y. Hou, Y.B. Huang, Y.L. Liang, et al., *CCS Chem.* 1 (2019) 384–395.
- [11] D. Chen, Y. Wang, D. Liu, et al., *Carbon Energy* 2 (2020) 443–451.
- [12] J.D. Yi, R. Xie, Z.L. Xie, *Angew. Chem. Int. Ed.* 59 (2020) 23641–23648.
- [13] S. Gao, Y. Lin, X. Jiao, et al., *Nature* 529 (2016) 68–71.
- [14] W. Zhang, Y. Hu, L. Ma, et al., *Adv. Sci.* 5 (2018) 1700275.
- [15] Q. Li, J. Fu, W. Zhu, et al., *J. Am. Chem. Soc.* 139 (2017) 4290–4293.
- [16] S. Zhao, D.W. Wang, R. Amal, L. Dai, *Adv. Mater.* 31 (2019) e1801526.
- [17] Z. Sun, T. Ma, H. Tao, Q. Fan, B. Han, *Chem* 3 (2017) 560–587.
- [18] X. Duan, J. Xu, Z. Wei, et al., *Adv. Mater.* 29 (2017) 1701784.
- [19] I.M. Hasan, L. Peng, J. Mao, *Carbon Energy* 3 (2021) 24–49.
- [20] D. Yi, D.H. Si, R. Xie, et al., *Angew. Chem. Int. Ed.* 60 (2021) 17108–17114.
- [21] C.W. Kung, C.O. Audu, A.W. Peters, et al., *ACS Energy Lett.* 2 (2017) 2394–2401.
- [22] I. Hod, M.D. Sampson, P. Deria, et al., *ACS Catal.* 5 (2015) 6302–6309.
- [23] L. Ye, J. Liu, Y. Gao, et al., *J. Mater. Chem. A* 4 (2016) 15320–15326.
- [24] Y. Wang, P. Hou, Z. Wang, P. Kang, *ChemPhysChem* 18 (2017) 3142–3147.
- [25] C. He, Q.J. Wu, M.J. Mao, et al., *CCS Chem.* 2 (2020) 2368–2380.
- [26] S. Dou, J. Song, S. Xi, et al., *Angew. Chem. Int. Ed.* 58 (2019) 4041–4045.
- [27] Z. Xin, J. Liu, X. Wang, et al., *ACS Appl. Mater. Interfaces* 13 (2021) 54959–54966.
- [28] Y.R. Wang, Q. Huang, C.T. He, et al., *Nat. Commun.* 9 (2018) 4466.
- [29] C. He, J. Liang, Y.H. Zou, *Natl. Sci. Rev.* (2022) nwab157.
- [30] G. Paille, M. Gomez-Mingot, C. Roch-Marchal, et al., *J. Am. Chem. Soc.* 140 (2018) 3613–3618.
- [31] B. Wang, W. Li, Z. Liu, et al., *RSC Adv.* 10 (2020) 12129–12134.
- [32] X. Yuan, Q. Mu, S. Xue, et al., *J. Energy Chem.* 60 (2021) 202–208.
- [33] Y.N. Gong, L. Jiao, Y. Qian, et al., *Angew. Chem. Int. Ed.* 59 (2020) 2705–2709.
- [34] L. Song, T. Li, S. Zhang, *J. Phys. Chem. C* 121 (2016) 293–299.
- [35] M. Sathish, K. Miyazawa, *Molecules* 17 (2012) 3858–3865.
- [36] W. Kratchmer, *Nature* 347 (1990) 354–358.
- [37] Y. Wei, M. Ma, W. Li, et al., *Appl. Catal. B: Environ.* 238 (2018) 302–308.
- [38] K.A. Affholter, S.J. Henderson, G.D. Wignall, et al., *J. Chem. Phys.* 99 (1993) 9224–9229.
- [39] C. Li, X. Liu, P. Huo, Y. Yan, et al., *Small* 17 (2021) e2102539.
- [40] X. Kang, Q. Zhu, X. Sun, et al., *Chem. Sci.* 7 (2016) 266–273.
- [41] S. Hermes, F. Schröder, S. Amirjalayer, R. Schmid, R.A. Fischer, *J. Mater. Chem.* 16 (2006) 2464–2472.
- [42] S. Hermes, M.K. Schroter, R. Schmid, et al., *Angew. Chem. Int. Ed.* 44 (2005) 6237–6241.
- [43] W. Morris, B. Voloskiy, S. Demir, et al., *Inorg. Chem.* 51 (2012) 6443–6445.
- [44] F.J.M. Hoeben, P. Jonkheijm, E.W. Meijer, A.P.H.J. Schenning, *ChemInform* 105 (2005) 1491–1546.
- [45] C. Zhang, H. Li, C. Li, et al., *Molecules* 25 (2019) 168.
- [46] K. Vimalanathan, R.G. Shrestha, Z. Zhang, et al., *Angew. Chem. Int. Ed.* 56 (2017) 8398–8401.
- [47] M.D. Zhang, D.H. Si, J.D. Yi, et al., *Small* 16 (2020) e2005254.
- [48] U. Takashi, H. Satoshi, K. Kana, et al., *J. Am. Chem. Soc.* 130 (2008) 6781–6788.
- [49] A.M. Limaye, J.S. Zeng, A.P. Willard, K. Manthiram, *Nat. Commun.* 12 (2021) 1–10.
- [50] J.P. Hare, H.W. Kroto, R. Taylor, *Chem. Phys. Lett.* 589 (2013) 57–60.
- [51] B. Ghanbari, M. Zarepour-jevinani, A.H. Mohammadzadeh, *J. Photochem. Photobiol. A* 418 (2021) 113414.
- [52] H. Cheng, X. Wu, M. Feng, et al., *ACS Catal.* 11 (2021) 12673–12681.
- [53] P. Bairi, K. Minami, W. Nakanishi, et al., *ACS Nano* 10 (2016) 6631–6637.
- [54] S. Onori, S. Montazeri, J. Inorg. Organometal. Polym. Mater. 31 (2021) 4222–4235.
- [55] X. Zhang, X. Ai, R. Zhang, et al., *Carbon* 106 (2016) 202–207.
- [56] P. Sharma, R. Singhal, R. Vishnoi, et al., *Vacuum* 123 (2016) 35–41.
- [57] J.B. Sundqvist, *Diam. Relat. Mater.* 73 (2017) 143–147.